Cancer Pathogenesis and Therapy 1 (2023) 98–110

Contents lists available at ScienceDirect

Cancer Pathogenesis and Therapy

journal homepage: www.journals.elsevier.com/cancer-pathogenesis-and-therapy

Research article

Dachaihu decoction inhibits hypernutrition-induced liver metastasis from colorectal cancer by maintaining the gut vascular barrier

Ruolei Wang [a,1], Fengjing Jia [a,1], Zhenguo Zhao [b], Liqing Du [a], Lianheng Lu [a], Dongkui Xu [c,**], Feng He [a,*]

[a] The Center for Cancer Research, Academy of Integrative Medicine, Shanghai University of Traditional Chinese Medicine, Shanghai 201203, China
[b] Department of Orthopaedics, National Cancer Center/National Clinical Research Center for Cancer/Cancer Hospital, Chinese Academy of Medical Sciences and Peking Union Medical College, Beijing 100021, China
[c] VIP Department, National Cancer Center/National Clinical Research Center for Cancer/Cancer Hospital, Chinese Academy of Medical Sciences and Peking Union Medical College, Beijing 100021, China

HIGHLIGHTS

- Hypernutrition or high-fat diet (HFD) uptake promotes liver metastasis in colorectal cancer (CRC) by disrupting the gut vascular barrier (GVB).
- Dachaihu decoction (DCHD) ameliorates HFD-induced hyperlipidemia and aberrant bile acid metabolism that disrupt the integrity of GVB.
- DCHD inhibits the spread of CRC cells to the systemic circulation by decreasing the aberrant bile acids-induced GVB leakage.
- DCHD inhibits intracellular Ca^{2+} elevation and reactive oxygen species (ROS) accumulation induced by aberrant bile acids to maintain homeostasis.

GRAPHICAL ABSTRACT

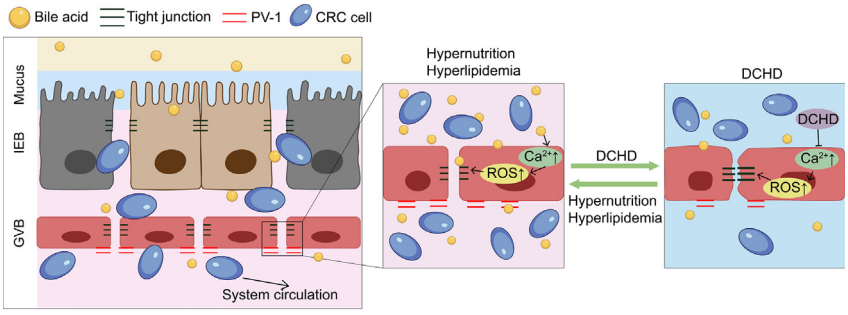

GVB disruption by hypernutrition and its maintenance by DCHD in CRC metastasis

CRC:Colorectal cancer; IEB:Intestinal epithelial barrier; GVB:Gut vascular barrier; DCHD: Dachaihu Decoction; ROS:Reactive oxygen species.

ARTICLE INFO

Managing Editor: Peng Lyu

Keywords:
Colorectal cancer
Metastasis
Hypernutrition
Dachaihu decoction
Gut vascular barrier

ABSTRACT

Background: Colorectal cancer (CRC) is the third most common malignancy and the second deadliest cancer worldwide. Metastasis to the liver, the most common metastatic site in CRC, is the leading cause of death in patients with CRC. Hyperlipidemia, which is common in patients with CRC, promotes CRC progression and metastasis. Hyperlipidemia is commonly observed in obese patients and is often induced by hypernutrition. The underlying mechanism of hypernutrition-induced hyperlipidemia in promoting CRC liver metastasis remains unclear, and there is an unmet need for effective and low-cost treatments for patients with CRC.
Methods: A mouse cecum orthotopic CRC model combined with high-fat diet (HFD) feeding, was established to mimic liver metastasis in CRC in obese patients. The effects of Dachaihu decoction (DCHD), a traditional herbal

* Corresponding author: The Center for Cancer Research, Academy of Integrative Medicine, Shanghai University of Traditional Chinese Medicine, Shanghai 201203, China.
** Corresponding author: VIP Department, National Cancer Center/National Clinical Research Center for Cancer/Cancer Hospital, Chinese Academy of Medical Sciences and Peking Union Medical College, Beijing 100021, China.
E-mail addresses: 13691583382@163.com (D. Xu), fhe@shutcm.edu.cn (F. He).
[1] Ruolei Wang and Fengjing Jia contributed equally to this work.

https://doi.org/10.1016/j.cpt.2023.02.003
Received 29 December 2022; Received in revised form 25 February 2023; Accepted 28 February 2023

Reactive oxygen species
Oxidative stress

medicine used to treat inflammation and nonalcoholic fatty liver disease, and of the conventional prescription medicine obeticholic acid (OCA) were evaluated. HFD-induced obesity, hyperlipidemia, and CRC liver metastasis were assessed, along with the histology and pathology of the liver and intestine and the expression of metabolic genes in these tissues. The effects of DCHD and OCA on HFD-induced outcomes were evaluated, and human umbilical vein endothelial cells (HUVECs) treated with bile acids (BAs) and DCHD were used to study the underlying mechanisms *in vitro*.

Results: HFD-mediated obesity and hyperlipidemia promoted CRC metastasis, accompanied by disruption of the gut vascular barrier (GVB) and altered bile acid (BA) metabolism. DCHD decreased HFD-induced hyperlipidemia and liver metastasis in CRC, improving overall survival. Those effects of DCHD were equivalent to or better than those of OCA. DCHD regulated the expression of genes of BA metabolism and tight junctions (TJ) to prevent HFD-induced disruption of the GVB. In HUVECs, DCHD prevented the increases in intracellular Ca^{2+} and accumulation of reactive oxygen species induced by primary conjugated BAs, assisting in the maintenance of redox homeostasis and preventing the downregulation of TJ proteins, thereby maintaining the integrity of the endothelial barrier.

Conclusions: The data provide a link between hypernutrition and GVB disruption, which contributes to high liver metastasis in patients with CRC. DCHD may represent a novel therapy in CRC, and targeting abnormal lipid metabolism could be a promising therapeutic strategy for avoiding hypernutrition-associated CRC metastasis.

Introduction

Colorectal carcinoma is the leading malignant tumor of the digestive system and patients with late-stage colorectal cancer (CRC) liver metastasis have poor survival.[1,2] There are multiple etiological factors for CRC, including diet, lifestyle, and genetic susceptibility.[3–5] Hypernutrition, for example, in the form of a Western or high-fat diet (HFD) intake, along with a sedentary lifestyle, is associated with obesity and dyslipidemia, which in turn promote CRC tumorigenesis and progression.[6] Aberrant lipid metabolism is a hallmark of CRC, and obesity and hyperlipidemia are risk factors for CRC progression.[7] Patients with CRC and high blood lipid levels have a poor prognosis, including postoperative complications and distant metastasis.[8,9] Hyperlipidemia is a common metabolic disorder characterized by abnormal blood lipoproteins, including elevated total cholesterol (TC), triglycerides (TG), and low-density lipoprotein cholesterol (LDL-C).[10] Increased blood lipid levels affect the gut bacteria and the metabolism of cholesterol, fatty acids, and bile acids (BAs), leading to organelle dysfunction and generation of reactive oxygen species (ROS) and, ultimately, initiation and progression of tumors, including CRC.[6,11–13] ROS and stress response signaling are associated with CRC tumorigenesis and development through various mechanisms,[14,15] but the mechanism of CRC development induced by obesity and increases in blood lipids remains incompletely understood.

Many patients with CRC develop distant metastases within 5 years and the liver is the most common organ involved.[16] CRC liver metastasis involves a subset of CRC cells undergoing a series of events to escape the primary CRC, involving morphological changes such as epithelial-to-mesenchymal transition, local migration through the extracellular matrix, intravasation, survival in the vascular circulation, extravasation and colonization of the liver, to form a more aggressive secondary cancer.[17] Gut vascular barrier (GVB) disruption associated with intravasation is critical for the metastasis of CRC primary tumor cells to the liver,[18] and aberrant lipid metabolism has been implicated in vascular damage. Besides TG and cholesterol, BAs also contribute to GVB disruption.[19] We hypothesized that reduction in blood lipid levels is beneficial for maintaining or restoring the GVB, thereby inhibiting CRC liver metastasis. Atorvastatin and obeticholic acid (OCA) have been shown to be beneficial in the treatment of lipid metabolic disorder,[6,20,21] but traditional medicine, which has been used for thousands of years and is increasingly recognized worldwide, may also offer solutions. Many phytochemicals are obtained from herbal medicines, including traditional medicines commonly used in China, Japan, India, and other parts of the world.[22] The World Health Organization Global Centre for Traditional Medicine estimates that 170 member states and around 80% of the world's population use and benefit from traditional medicine. Over 40% of existing pharmaceutical formulations are based on natural products, and landmark drugs, including aspirin and artemisinin, originated from traditional medicines.[23] Dachaihu decoction (DCHD), a classical, traditional Chinese formula first recorded in the *Treatise on Febrile Disease* (*Shang Han Za Bing Lun*) by Zhongjing Zhang, has been increasingly applied in the treatment of conditions including hyperlipidemia due to its preventive and therapeutic effects with limited side effects, as well as low cost.[24,25] DCHD has also been shown to have significant beneficial effects in type 2 diabetes mellitus[26] and nonalcoholic fatty liver disease.[27,28]

Consumption of an HFD induces obesity and hyperlipidemia, which increases the risk of many cancers. Our previous studies have shown that HFD promotes the development of nonalcoholic fatty liver disease and liver tumorigenesis and progression.[13,29] To understand how hyperlipidemia promotes liver metastasis in CRC and whether a potential lipid-lowering herbal medicine, DCHD, could be used in clinical therapy for CRC, we generated an orthotopic HFD-fed CRC mouse model to study hypernutrition-induced hyperlipidemia and its effects on CRC progression and liver metastasis in the presence and absence of DCHD. We aimed to assess the effect of DCHD on blood lipid concentrations in mice as well as hyperlipidemia-induced liver metastasis in CRC. Separately, we aimed to assess the effects of DCHD on the GVB following disruption by HFD and compare the effects of DCHD to those of the conventional prescribed medicine OCA.

Methods

Mouse experiments

Five-week-old male C57BL/6 mice were purchased from Shanghai Jihui Laboratory Animal Co. Ltd (Shanghai, China). Mice were fed normal chow (NC) or an HFD (FB-D12492, 60% fat, Wuxi Fanbo Biotechnology, Wuxi, China) from 6 weeks of age until sacrifice. For the hyperlipidemia rescue experiment, HFD-fed mice were administered vehicle control, the farnesoid X receptor (FXR) agonist OCA (30 mg/kg, SML3096, Sigma-Aldrich, St Louis, MO, USA) or DCHD (5, 10, or 20 g/kg body weight), by oral gavage daily for 4 weeks before blood and tissue collection. For liver metastasis, a CRC cecum orthotopic model was used as previously described.[30,31] Briefly, a mouse with a CRC xenograft derived from previous subcutaneous implantation of 1×10^7 murine MC-38 CRC cells was euthanized. The xenograft tumor was removed and cut into pieces of about 1 mm^3. Host mice were anesthetized with isoflurane and disinfected, and the cecal wall was mildly damaged to facilitate tumor cell infiltration. Tumor pieces were implanted into the serous layer of the cecum with medical OB glue (Yiyongwenhexing, Guangzhou, China), then the cecum was returned to the abdomen, and the abdomen was closed with sutures.

In a separate experiment, mice were intragastrically administered conjugated bile acids (C-BA, taurocholic acid [TCA], taurochenodeoxycholic acid [TCDCA], glycocholic acid [GCA], and

glycochenodeoxycholic acid [GCDCA]) 30 mg/kg for 4 weeks prior to testing GVB function in an intestinal loop experiment. Mice were maintained in filter-topped cages on autoclaved food and water on a 12-h light/dark cycle at a housing temperature of 22 °C-25 °C and a humidity of 60%. Mice were randomized in individual experiments (n = 3–10 per group).

Blood cholesterol and triglyceride assays

Blood TC, TG, and LDL-C were analyzed using commercial kits (cat# A111-1-1, A110-1-1, and A113-1-1, respectively) from the Nanjing Jiancheng Bioengineering Institute (Nanjing, China) according to the manufacturer's protocol.

Preparation of Dachaihu decoction

The DCHD formula used in this study was in accordance with the record in *Treatise on Febrile Disease* by Zhongjing Zhang. This formula consisted of 12 g Radix Bupleuri, 9 g Radix Scutellariae, 9 g Rhizoma Pinelliae, 9 g *Paeonia lactiflora*, 9 g Fructus Aurantii Immaturus, 9 g *Rheum palmatum* L., 15 g Rhizoma Zingiberis Recens, and 10 g *Ziziphus jujube* Mill. All herbs were purchased from the Shanghai Shuguang Hospital. The components of DCHD were extracted twice in boiling distilled water (300 mL) for 1 h after soaking for 30 min. The decoction was filtered and boiled to reduce the volume to 85 mL to give a crude drug concentration of 1 g/mL. For the clinical dose of DCHD, body surface area was calculated based on a body weight of 30 g for mice and 70 kg for humans. The dosage of DCHD in mice was calculated with the dose set as medium (medium dose = 9.1 × 30/10.6 × 70,000 × 85 = 10 g/kg body weight). The low and high doses were set at 5 and 20 g/kg, respectively. DCHD doses were formulated in 100 μL saline and orally administered for 1 week before CRC cecum orthotopic implantation. The mice were continuously administered DCHD for 2 weeks, starting from day 3 post-surgery.

Fluorescein isothiocyanate-labeled-dextran permeability assay

For *in vivo* studies, mice fasted overnight were gavaged with 500 mg/kg Fluorescein-isothiocyanate-labeled (FITC)-dextran (4 kDa, #46944, Sigma-Aldrich). After 4 h, blood was collected from the retro-orbital sinus and centrifuged at 1000 g for 10 min at 4 °C to separate the plasma. FITC-dextran in plasma samples was measured by fluorescence intensity using a SPARK multimode Microplate Reader (Tecan, Männedorf, Sweden) with an excitation wavelength of 490 nm and an emission wavelength of 520 nm.

For *in vitro* studies, 1×10^5 human umbilical vein endothelial cells (HUVECs) were seeded in the upper chamber of a Transwell insert with a pore size of 0.4 μm in a 24-well plate. HUVECs were grown for 1 day until a monolayer formed. The cells were then treated with C-BA for 24 h, and the media in the Transwell insert and the bottom chamber were removed, and 150 μL of 0.1 mg/mL FITC-dextran and 500 μL of serum-free media were added to the Transwell upper chamber and the bottom well, respectively, and incubated at 37 °C for 4 h. Permeability to FITC-dextran was determined by the fraction of total FITC fluorescence intensity in the bottom well. Permeability=(fluorescence in bottom well)/[(fluorescence in top well) + (fluorescence in bottom well)].

Intestinal ligated loop assay

Mice were anesthetized with isoflurane, then 1 cm of the terminal ileum was ligated. A total of 4 mg of 4 kDa FITC-dextran in 100 μL sterile phosphate-buffered saline (PBS) was injected into the ligated loop. After 1 h, blood samples were collected from the retro-orbital sinus. Livers were fixed in Carnoy's fixative (60% ethanol, 30% chloroform, 10% glacial acetic acid) and embedded in paraffin blocks. Sections (5 μm) were stained with 4′,6-diamidino-2-phenylindole (DAPI). The number of FITC particles was observed at 40 × magnification using a fluorescence microscope (Zeiss, Axio7, Germany).

Quantitative reverse transcriptase polymerase chain reaction

Total RNA from HUVECs, mouse liver, or intestinal tissues was isolated using Trizol reagent (Beyotime) according to the manufacturer's instructions. Total RNA (1 μg) was reverse transcribed to cDNA using a Hifair III 1st Strand cDNA Synthesis SuperMix kit (Yeasen, Shanghai, China). cDNA was diluted and used for quantitative real-time polymerase chain reaction (qRT-PCR) with SYBR Green PCR Master Mix (Yeasen) in a StepOne Plus Real-Time PCR System (Applied Biosystems, Waltham, MA, USA). Relative mRNA expression was presented as arbitrary units and was calculated by the 2(ΔΔ CT) method. The primers used are given in Supplementary Table 1.

Immunofluorescence and confocal microscopy

Intestinal tissues were fixed overnight in 4% paraformaldehyde (PFA) at 4 °C, followed by dehydration in 30% sucrose for 4 h and embedded in optimal cutting temperature (OCT) compound. Immunofluorescence staining of tissue sections was performed as described previously.[32] Cryosections (8 μm) were rehydrated, blocked with blocking buffer (0.1 M Tris-HCl, 5% goat serum, 0.25% Triton X-100, pH 7.4), and stained with the following primary antibodies: anti-ZO-1 (ab221547, Abcam, Cambridge, UK, 1:250), anti-PV1 (PA5-115774, Invitrogen, Waltham, MA, USA, 1:250), and anti-CD34 (ab81289, Abcam, 1:250). Tissues were incubated with the appropriate fluorescent secondary antibodies. Nuclei were stained with DAPI (C1006, Beyotime, Shanghai, China). Images were captured using a TCS SP5 confocal microscope (Leica, Wetzlar, Germany). ImageJ software package was used for fluorescence quantification.

Cell culture

Mouse colon cancer cell line MC-38, human umbilical vein endothelial cells HUVECs, and colon cancer cell line HCT-116 stably expressing green fluorescent protein (GFP) were acquired from the Cell Bank of the National Collection of Authenticated Cell Cultures (Shanghai, China). MC-38 and HUVECs were cultured in Dulbecco's modified Eagle Medium (DMEM, Gibco, Billings, MT, USA), supplemented with 10% fetal bovine serum (FBS), penicillin (100 IU/mL), and streptomycin (100 μg/mL). HCT-116 cells were cultured in RPMI 1640 medium (Gibco) supplemented with 10% FBS. Cells were grown in a humidified chamber with 5% CO_2 at 37 °C.

Cancer cell transendothelial invasion assay

HUVECs (1×10^5 cells) were seeded in the upper chamber of a Transwell insert and grown for 1 day until a monolayer formed. The cells were then treated with 100 μM C-BAs for 24 h before the medium was changed to serum-free medium, and HCT-116 cells (5×10^4 cells) stably expressing GFP were placed on top of the HUVEC monolayer. The medium in the bottom well was DMEM supplemented with 10% FBS. HCT-116 cells were allowed to grow and migrate for 48 h at 37 °C prior to in-chamber fixation with 4% PFA and DAPI staining. Images were captured using a TCS SP5 confocal microscope (Leica) and quantified using ImageJ software.

Measurements of transendothelial electrical resistance

HUVECs (1×10^5 cells) were seeded into the upper chamber inserts of a Transwell plate and allowed to grow until a monolayer formed. Cells were treated with C-BAs for 24 h. The transendothelial electrical resistance (TEER) of the cell barrier was measured using a Millicell ERS-2 Epithelial Volt-Ohm meter (MilliporeSigma, Burlington, MA, USA). The

resistance of a blank well (membrane without cells) was recorded as a background reading and subtracted from measured resistance values. This value was multiplied by the membrane surface area (0.33 cm^2) to calculate the TEER. Each well was measured three times, and each experiment was performed in triplicate. TEER results are presented as the mean ± standard deviation (SD).

Western blotting

Mouse tissues were homogenized in RIPA buffer containing protease and phosphatase inhibitor cocktails (Beyotime) using a tissue homogenizer (Wonbio, Shanghai, China) according to the manufacturer's instructions. Cells were lysed in RIPA buffer (P0013B, Beyotime) containing protease and phosphatase inhibitor cocktails (P1049, Beyotime). After centrifugation, the supernatants were collected and quantified using a bicinchoninic acid (BCA) protein assay kit (P0011, Beyotime). Protein lysates were separated using sodium dodecyl sulfate-polyacrylamide gel electrophoresis (20325ES62, Yeasen), transferred to 0.45 μm polyvinylidene difluoride membranes (Millipore, Burlington, MA, USA), blocked in 5% nonfat milk in PBS plus Tween-20 (0.1% [v/v]) buffer, and incubated with primary antibodies at 4 °C overnight. The blot was incubated with secondary antibodies for 1 h, and detection used Clarity Western ECL Substrate (Biorad, Hercules, CA, USA) with imaging using a Tanon fluorescence imaging system. ImageJ software package was used for densitometry analysis, and band density was normalized to β-actin expression. Antibody details were: anti-ZO-1 (ab190085, Abcam, 1:5000), anti-occludin (ab216327, Abcam, 1:5000), anti-claudin-1 (ab242370, Abcam, 1:5000), and anti-β-actin (3700, Cell Signaling Technology, 1:5000).

Fluo-4 AM Ca^{2+} staining

HUVECs were seeded in 6-well plates at 2×10^5 cells/well. After treatment, cells were washed with PBS three times and incubated with 2 μmol/L cell-permeant Ca^{2+} probe Fluo-4 AM (Beyotime) in Hank's Balanced Salt Solution (HBSS) for 30 min at 37 °C. The cells were then washed three times with PBS and incubated with 10 μg/ml Hoechst 33342 (HY-15559A, MedChemExpress, Princeton, NJ USA) for 10 min at 37 °C. Live cell images were captured using a Zeiss Axio7 microscope, and images were acquired using ZEN image software. ImageJ software package was used for quantification.

Reactive oxygen species staining

HUVECs were seeded in 6-well plates (2×10^5 cells) overnight before treatment with the different drugs (GCDCA 100μM, DCHD 20 μg/mL). After treatment, the cells were incubated with 5 μmol/L cell-permeant 2′,7′-dichlorodihydrofluorescein diacetate (H2DCFDA) (HY-D0940, MedChemExpress) in HBSS for 60 min at 37 °C, followed by three PBS washes and incubation with 10 μg/mL Hoechst 33342 for 10 min at 37 °C. Live cell images were captured by using a Zeiss LSM 710 confocal microscope.

ROS staining of tissues with dihydroethidium (DHE) was performed as previously described.[29] Briefly, intestinal tissues were embedded in OCT compound (4583, Sakura, Tokyo, Japan) without fixing. Cryosections (8 μm) were washed in PBS for 1 min and then incubated with 3 μmol/L DHE (C3807, Apexbio Technology, Houston, TX, USA) at 37 °C for 30 min, followed by three 5-min washes in PBS in the dark. The stained slides were counterstained with DAPI and mounted immediately in VECTASHIELD (H-1200, Vector Laboratories, Burlingame, CA, USA). Images were captured using a TCS SP5 confocal microscope (Leica). ImageJ software package was used for fluorescence quantification.

Statistical analysis

GraphPad Prism 8.0.2 (GraphPad Software, Boston, MA, USA) was used for statistical analysis and graphing. Statistical significance was determined using the one-way analysis of variance with Dunnett's post-hoc analysis. All data are shown as mean ± SD. P values < 0.05 were considered statistically significant.

Results

High-fat diet feeding induces hyperlipidemia and promotes liver metastasis in colorectal cancer, but Dachaihu decoction counteracts these effects

HFD is a dietary regimen rich in fat (60% of energy intake), known to induce obesity and hyperlipidemia in C57BL/6 mice.[13,29,33] To understand whether high serum lipid levels induced by HFD exacerbate CRC primary tumor metastasis to the liver, we fed mice with NC or HFD for 8 weeks before orthotopic implantation of MC-38 CRC cells into the cecum and continued NC or HFD feeding until sample harvesting. Consistent with previous reports,[13,29] HFD feeding induced hyperlipidemia, comprising increased levels of blood TC, TG, and LDL-C [Figure 1A] as well as body weight gain [Supplementary Figure 1A]. Importantly, mice with hyperlipidemia displayed a significantly higher number of tumor nodules in the liver metastasized from colons than did paired NC-fed mice [Figures 1B and C]. To determine whether the well-known herbal medicine DCHD has beneficial effects on CRC liver metastasis and HFD-induced hyperlipidemia, HFD-fed mice were orthotopically implanted with MC-38 cells in the cecum to mimic CRC metastasis. Mice were intragastrically administered different doses of DCHD, low-dose DCHD (L-DCHD, 5 g/kg), medium-dose DCHD (M-DCHD, 10 g/kg), and high-dose DCHD (H-DCHD, 20 g/kg), as well as positive control OCA, the first FDA-approved FXR-targeting drug for primary biliary cholangitis patients.[34] As with OCA, DCHD decreased serum TC, TG, and LDL-C levels, especially at medium and high doses [Figure 1D]. DCHD treatment also showed a tendency to delay body weight gain [Supplementary Figure 1B]. DCHD treatment decreased the number of liver nodules and prolonged the overall survival (OS) of HFD-fed mice orthotopically implanted with CRC cells in the cecum [Figures 1E and F, Supplementary Figure 1C]. The data indicate that in parallel with decreasing blood lipid levels, DCHD inhibited HFD-induced liver metastasis in CRC.

Dachaihu decoction decreases high-fat diet-induced intestinal barrier disruption and gut vascular barrier leakage

Previous studies showed that mice fed with HFD for 1 week displayed changes in gut barrier morphology.[35] To evaluate how HFD affects intestinal homeostasis, we first analyzed the morphology of the ileum and colon from NC- and HFD-fed mice. Hematoxylin and eosin (H&E) and Alcian blue staining were used to determine intestinal morphology. Consistent with a previous report,[35] HFD-induced disruption of intestinal villi and crypt morphology was alleviated by oral administration of DCHD [Supplementary Figure 2A]. The number of goblet cells increased in the DCHD-treated groups, suggesting that DCHD enables repair of the intestinal barrier [Supplementary Figure 2B]. The results indicate that DCHD has a good therapeutic capability to repair gut morphological damage induced by HFD feeding.

GVB disruption facilitates the entry of CRC tumor cells into blood vessels that converge on the portal vein, leading to liver metastasis.[18] We reasoned that DCHD might lower GVB permeability and thereby decrease the number of metastatic lesions in CRC of HFD-fed mice. First, we assessed GVB permeability by challenging mice with 4 kDa FITC-dextran. We measured the fluorescence intensity of serum FITC-dextran 4 h after FITC-dextran administration. DCHD treatment at all three doses reduced GVB leakage in HFD-fed mice [Figure 2A]. To confirm the DCHD-induced amelioration of GVB disruption, we analyzed the expression of genes encoding tight junction (TJ) proteins, including Claudin, Occludin, and

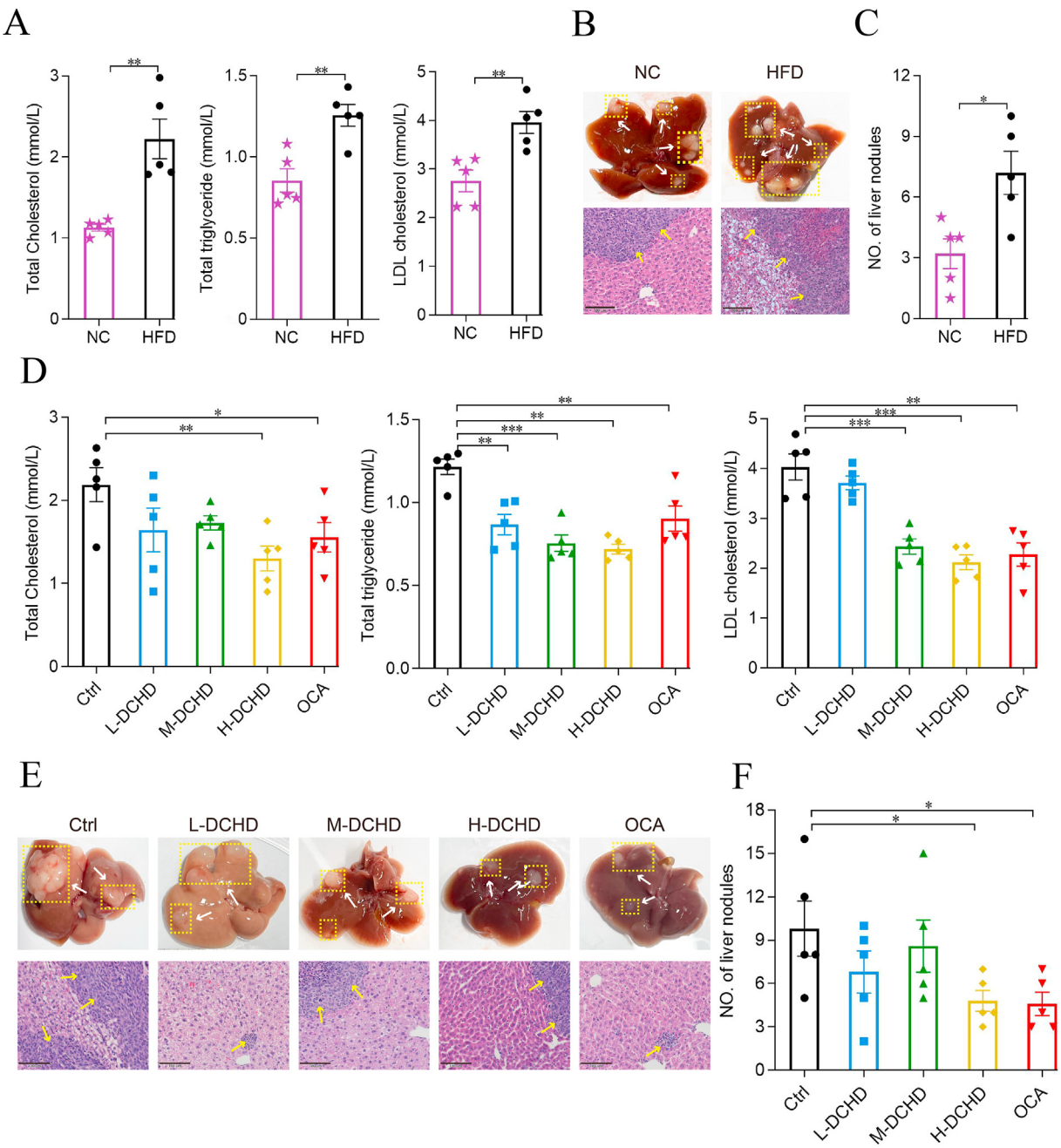

Figure 1. A high-fat diet induces hyperlipidemia and liver metastasis in colorectal cancer, but Dachaihu decoction counteracts these effects. (A) Serum total cholesterol, triglycerides, and LDL-cholesterol in NC- and HFD-fed mice orthotopically implanted with MC-38 CRC cells in the cecum. (B) Top, macroscopic appearance of livers with metastasized CRC tumor nodules in NC- and HFD-fed mice. Dotted squares and White Arrows indicate metastatic tumors. Bottom, H&E staining of livers. Yellow arrows indicate tumor regions. Scale bar, 100 μm. (C) Number of metastasized liver nodules in mice. (D) Serum lipids in HFD-fed mice orally administrated vehicle control (Ctrl), DCHD at low (L-DCHD), medium (M-DCHD) or high (H-DCHD) dose or positive control OCA. (E) Top, macroscopic appearance of livers with metastasized CRC tumor nodules following OCA or DCHD treatment. White arrows indicate metastatic tumors. Bottom, H&E staining of livers. Yellow arrows indicate tumor regions. Scale bar, 100 μm. (F) Number of metastasized liver nodules in mice following OCA or DCHD treatment. Mean ± SD ($n = 5$); *$P < 0.05$, **$P < 0.01$, ***$P < 0.001$.CRC: Colorectal cancer; DCHD: Dachaihu decoction; H&E: Hematoxylin and eosin; HFD: High-fat diet; LDL: Low-density-lipoprotein; NC: Normal-chow; OCA: Obeticholic acid; SD: Standard deviation.

ZO-1, in ileum and colon of HFD-fed mice with or without DCHD treatment. Plasmalemma vesicle-associated protein-1 (PV1) and vascular endothelial growth factor A (VEGFA) are considered markers of blood permeability.[36] DCHD treatment increased the expression of *Claudin* and *ZO*-1 mRNAs in both colon and ileum, with effects generally superior to those of OCA [Figure 2B, Supplementary Figure 2C]. Although there were no significant changes in the expression of *Occludin* in the colon, a low dose of DCHD increased *Occludin* expression in the ileum [Figure 2B, Supplementary Figure 2C]. The expression of *Pv1* and *Vegfa* were decreased, suggesting a decrease in vascular permeability in the colon and ileum of DCHD-treated mice [Figure 2B, Supplementary Figure 2C]. At a protein level, immunofluorescence staining for ZO-1 and PV-1 proteins showed that DCHD treatment increased the mean fluorescence intensity (MFI) of ZO-1 but decreased the MFI of PV-1 in the colon [Figures 2C–F] and ileum [Supplementary Figures 3A–3D] of mice. The effects of high DCHD on ZO-1 and PV-1 expression were similar to those

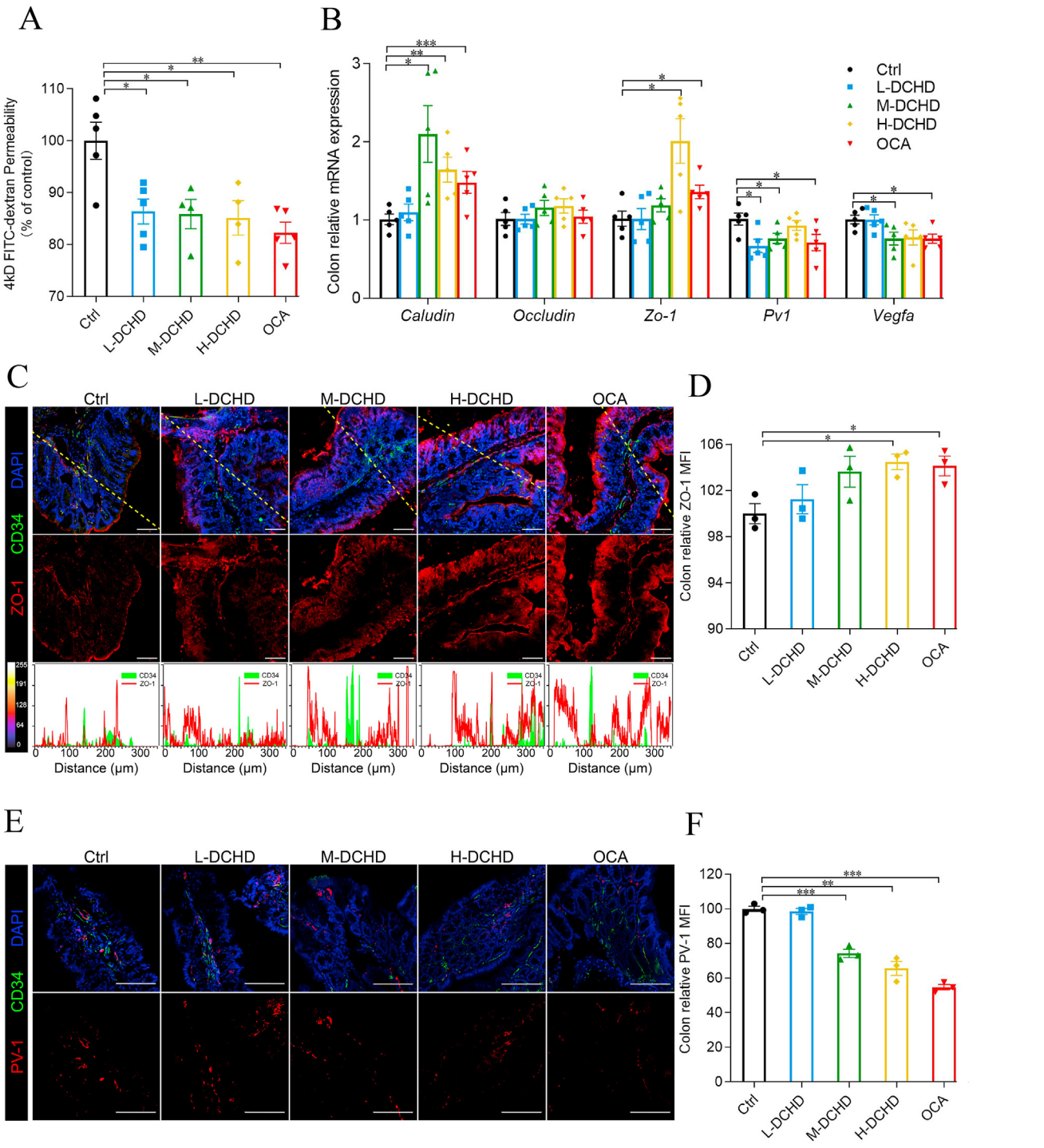

Figure 2. Dachaihu decoction prevents gut vascular barrier leakage in high-fat diet-fed mice. (A) Serum fluorescence intensity of FITC-dextran 4 h after administration in HFD-fed orthotopic CRC-bearing mice. Mean ± SD ($n = 5$) $^{*}P < 0.05$, $^{**}P < 0.01$, $^{***}P < 0.001$. (B) qRT-PCR analysis of relative mRNA expression of GVB permeability biomarkers in mouse colon, including TJ (*Claudin*, *Occludin*, and *ZO-1*) and vascular markers (*Pv1* and *Vegfa*). (C) Immunostaining of ZO-1 (red) and CD34 (green), and DNA staining (blue) in frozen sections of the colon. Top, merged images with a dotted line showing where fluorescence intensity was quantified. Middle, ZO-1 staining. Bottom, relative fluorescence intensity profiles for each protein. (D) Quantification of MFI for ZO-1. $^{*}P < 0.05$, $^{**}P < 0.01$, $^{***}P < 0.001$. (E) Immunostaining of PV-1 (red) and CD34 (green), and DNA staining (blue) in colon sections. Scale bar, 50 μm. (F) Quantification of MFI for PV-1. Mean ± SD ($n = 5$); $^{*}P < 0.05$, $^{**}P < 0.01$, $^{***}P < 0.001$.CRC: Colorectal cancer; FITC: fluorescein-isothiocyanate-labeled; GVB: Gut vascular barrier; HFD: High-fat diet; MFI: Mean fluorescence intensity; qRT-PCR: Quantitative real-time polymerase chain reaction; SD: Standard deviation; TJ: Tight junction.

of OCA. Liver metastasis in CRC involves intravasation of CRC into the portal vein at the primary tumor site, movement of CRC cancer cells into the circulation, and extravasation of circulating cancer cells into the liver for colonization. The liver is one of the most favorable target organs for tumor cell metastasis. Liver sinusoidal endothelial cells (LSECs) are highly specialized endothelial cells that contain many small pores or fenestrations that facilitate the transfer of substrates between the blood and liver parenchyma. LSECs contribute to liver tumor metastasis.[37] Whether DCHD also affects the morphology of the liver sinusoids may contribute to the outcome of CRC liver metastasis. We did not observe

changes in the morphology of liver sinusoids, as evidenced by CD34 staining [Supplementary Figures 3E and 3F], suggesting little or no effects of DCHD. Interestingly, immunofluorescence staining of ZO-1 in the liver showed that DCHD restored ZO-1 expression that was inhibited by HFD feeding [Supplementary Figures 4A–4D], suggesting an additional beneficial role of DCHD in maintaining the function of LSECs. ZO-1 is not expressed exclusively in the tight junctions of LSECs but is also expressed in paracellular hepatocytes around the lumen of bile canaliculi.[38] The effect of DCHD on the permeability of LSECs needs to be further studied. Overall, the findings suggest that DCHD inhibits HFD-induced liver metastasis in CRC by restoring GVB integrity and the integrity of liver sinusoids.

Dachaihu decoction protects against high-fat diet-induced gut vascular barrier disruption by alleviating aberrant conjugated bile acid metabolism

High blood levels of TG, cholesterol, and the cholesterol derivatives, bile acids (BAs), which are exclusively synthesized from cholesterol in the liver, are common in obesity. In addition to TG and cholesterol, BAs and aberrant BA metabolism contribute to CRC development and metastasis.[39,40] HFD elevates blood TG and cholesterol, which are transported into the liver, where cholesterol is metabolized to BAs, leading to metabolic perturbations.[6,41] DCHD decreased the levels of blood TG and cholesterol, as shown in Figure 1D. To understand the factors that are modulated by DCHD to reduce HFD-induced GVB disruption and CRC liver metastasis, we tested the effects of DCHD on BA metabolism. qRT-PCR analysis of gene expression in BA metabolism revealed that of the tested doses of DCHD, at least one dose level reduced liver expression of *Cyp7a1*, *Cyp8b1a*, *Cyp27a1*, *Cyp7b1*, bile acid-CoA synthetase (*Bacs*), and bile acid-CoA amino acid N-acyltransferase (*Baat*) involved in BA synthesis [Figure 3A]. In addition, the expression of sodium/taurocholate co-transporting polypeptide (*Ntcp*) and the bile salt export pump (*Bsep*), which are required for hepatic BA secretion and uptake, respectively, was decreased on DCHD treatment [Figure 3A]. The ileum of DCHD-treated HFD-fed mice showed lower levels of expression of apical sodium-dependent BA transporter (*Asbt*), multidrug resistance-associated protein 2 (*Mrp2*), *Mrp3*, and organic solute transporter subunit α/β (*Osta* and *Ostb*) responsible for BA absorption and secretion into the circulation by the terminal ileum enterocytes [Figure 3B]. Consistent with this, the expression of the FXR and its targets *Fgf15* and *Shp* were elevated in the ileum of DCHD-treated mice [Figure 3B]. In particular, genes associated with primary C-BAs, *Baat*, *Bacs*, and *Ntcp*, were downregulated by DCHD administration. Primary C-BAs have been shown to have adverse effects on CRC progression.[11,40] To confirm that C-BAs play a role in HFD-induced GVB disruption, four primary C-BAs, TCA, TCDCA, GCA, and GCDCA, were intragastrically administered to mice for 4 weeks, and GVB permeability was then analyzed by an intestinal loop experiment in which FITC-dextran was injected into the terminal ileum, to assess intestinal FITC-dextran absorption and passage to the liver. In livers of DCHD-treated mice, the fluorescent area of FITC-dextran in liver sections was higher compared with that in control mice, especially after treatment with TCA, TCDCA, and GCDCA [Figures 3C and D], indicating that the GVB is disrupted by these primary C-BAs. In parallel, the serum fluorescence intensity of FITC-dextran increased [Figure 3E]. In a parallel experiment, HUVECs were used to observe C-BA-induced barrier impairment. As expected, treatment with C-BAs significantly increased the permeability of HUVEC monolayers to FITC-dextran [Figure 3F] and decreased TEER [Figure 3G]. The data suggest that primary C-BAs, especially TCA, TCDCA, and GCDCA, disrupt the GVB.

Dachaihu decoction inhibits human umbilical vein endothelial cell barrier disruption and transendothelial invasion of colorectal cancer cells induced by conjugated bile acids

Given that C-BAs significantly increased GVB barrier permeability *in vivo* and HUVEC barrier permeability *in vitro*, we selected GCDCA to induce disruption of the HUVEC barrier and tested the effects of DCHD on GCDCA-induced disruption. DCHD treatment reversed permeability changes seen with FITC-dextran and changes in TEER induced by GCDCA [Figures 4A and B]. GCDCA decreased the expression of claudin, occludin, and ZO-1 both at the mRNA and protein levels, while DCHD generally reversed this effect, although the increase in ZO-1 protein did not reach significance [Figures 4C–E]. Similarly, the GCDCA-induced increase in PV-1 mRNA expression was suppressed by DCHD treatment [Figure 4C]. To further model CRC cell crossing of the GVB and disseminating via the hematogenous route, we used a transendothelial invasion assay to test the effects of DCHD on tumor cell migration. As expected, GCDCA-induced HUVEC barrier disruption increased the migration of tumor cells, but DCHD treatment decreased the number of migrating tumor cells [Figures 4F and G]. Increased movement of tumor cells across the endothelial monolayer could be due to an increased migratory ability, so to rule out the possibility of DCHD effects on MC-38 cell migration, we carried out an *in vitro* migration (wound-healing) assay. The results showed that DCHD did not affect the migration of MC-38 cells in a wound-healing context [Supplementary Figures 5A and 5B]. Interestingly, DCHD increased the migration of another CRC cell line, HCT-116 [Supplementary Figures 5C and 5D], suggesting a cell-specific effect of DCHD in cancer cell invasion. Together with the *in vivo* data, the results suggest that DCHD reverses HFD-induced increases in GVB permeability by regulating C-BA metabolism.

Dachaihu decoction induces expression of tight junction proteins by modulating Ca^{2+} and reactive oxygen species signaling

The expression of TJ was strongly associated with Ca^{2+} channels. Toxic factors often trigger endoplasmic reticulum (ER) stress, leading to the release of Ca^{2+} into the cytoplasm, which in turn decreases the expression of TJ proteins.[42] C-BAs induce Ca^{2+} release from the ER, contributing to intracellular Ca^{2+} overload.[43] To test whether DCHD regulates TJ expression and restoration of the vascular barrier through the regulation of Ca^{2+}, we stained HUVECs with a Ca^{2+} probe and a ROS indicator at early time points. In contrast to conventional gene expression changes occurring at 24 h after drug treatment, we found that GCDCA increased intracellular levels of Ca^{2+} and ROS at 3 h after treatment, but both levels were significantly decreased by DCHD [Figures 5A–D]. The findings indicate that DCHD inhibited GCDCA-triggered ER stress or oxidative stress, as evidenced by ER Ca^{2+} release and ROS generation. ROS generation is an important factor in stress responses and intestinal barrier homeostasis.[44] Glutathione metabolism is an important cellular oxidative stress response program.[15] We assessed the expression of genes of glutathione synthesis and utilization in HUVECs under single or combined treatment with GCDCA and DCHD. GCDCA increased glutathione synthetase (*GSS*) and glutathione S-transferase P (*GSTP*) mRNA levels, but this increase was suppressed by DCHD [Figure 5E]. A similar effect was observed for NAD(P)H quinone dehydrogenase 1 (*NQO1*), a protective antioxidant regulating oxidative stress [Figure 5E]. NQO1 is a transcription target of the master oxidative stress transcription factor, nuclear factor erythroid 2-related factor 2 (*NFE2L2*, encoding NRF2 protein).[32,45] We also stained intestinal tissues with the ROS indicator DHE and found that DCHD significantly decreased cellular ROS accumulation in both colon and ileum of DCHD-treated HFD-fed mice [Figures 6A–D]. DCHD reduced expression of *Gss* and *Gstp* in the ileum of HFD-fed mice, but not *Gclc* or *Nfe2l2* [Figure 6E], likely due to the presence of mixed cell types in the isolated tissues. These data suggest that DCHD decreases ER Ca^{2+} release and ROS accumulation and that these signals may trigger the GVB changes induced by HFD feeding.

Discussion

There is accumulating evidence that obesity and hypernutrition increase the risk of cancer. Specifically, CRC progression has been ascribed

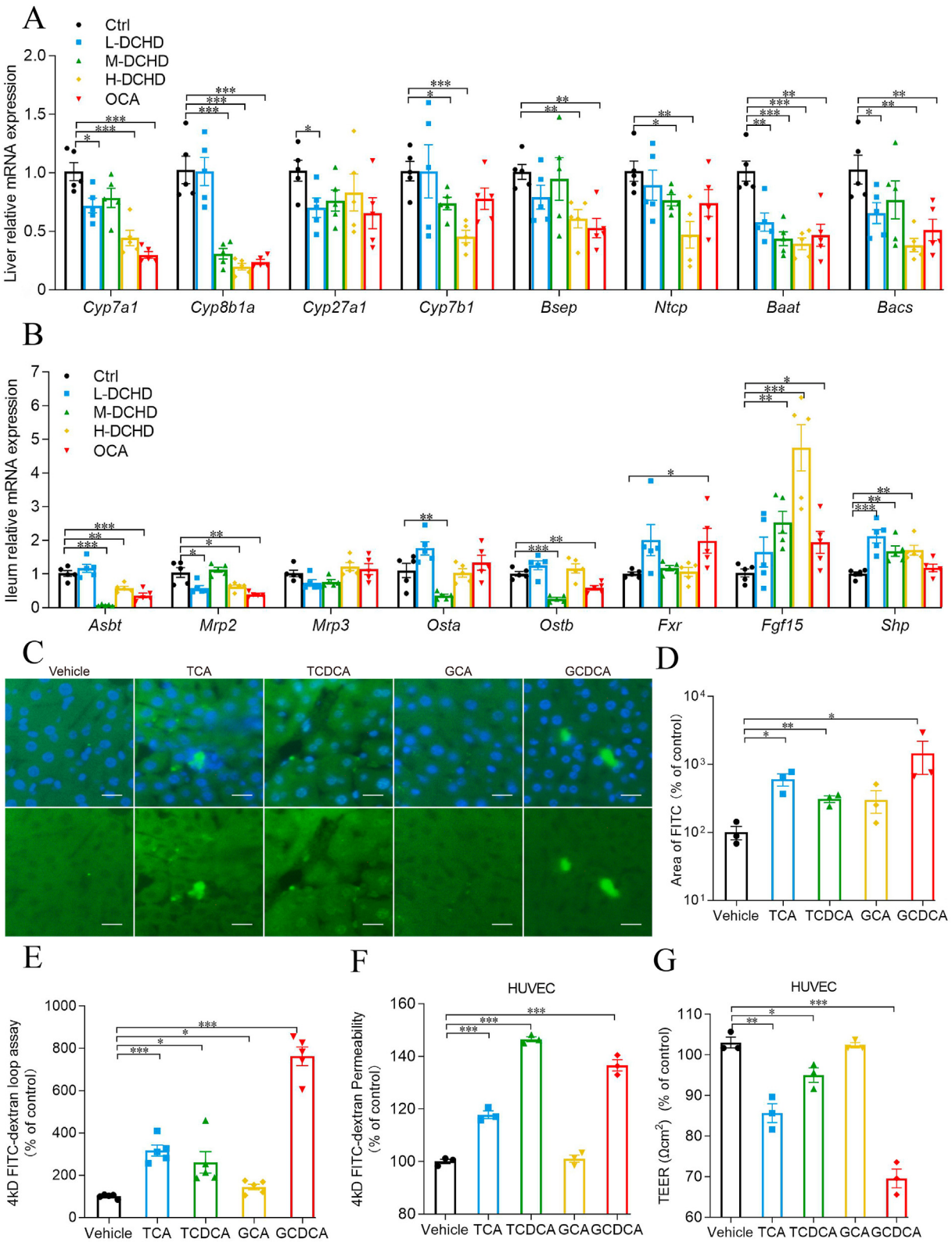

Figure 3. Dachaihu decoction modulates bile acid metabolism to alleviate high-fat diet-induced gut vascular barrier disruption. (A) qRT-PCR analysis of expression of genes involved in BA synthesis and transport in livers of HFD-fed orthotopic CRC-bearing mice. (B) qRT-PCR analysis of ileal expression of genes involved in BA absorption and secretion. (C) Fluorescence images of FITC-dextran (green) and DNA staining (blue). (D) Quantitation of FITC intensity in liver 1 h after FITC-dextran administration. Scale bar, 50 μm. (E) Serum fluorescence intensity of FITC-dextran in mice 1 h after intestinal loop instillation. (F) FITC-dextran permeability assay in HUVECs treated with 100 μmol/L primary (C-BAs, TCA, TCDCA, GCA, or GCDCA) or vehicle control. Permeability is given as a percentage FI in the lower well. (G) TEER in HUVECs grown with C-BAs; results from 3 independent experiments. Mean ± SD, $^{*}P < 0.05$, $^{**}P < 0.01$, $^{***}P < 0.001$.BA: Bile acid; C-BAs: conjugated bile acids; CRC: Colorectal cancer; FI: Fluorescence intensity; FITC: Fluorescein-isothiocyanate-labeled; GCA: Glycocholic acid; GCDCA: Glycochenodeoxycholic acid; GVB: Gut vascular barrier; HFD: High-fat diet; HUVECs: Human umbilical vein endothelial cells; MFI: Mean fluorescence intensity; qRT-PCR: Quantitative real-time polymerase chain reaction; SD: Standard deviation; TCA: Taurocholic acid; TCDCA: Taurochenodeoxycholic acid; TEER: Transepithelial electrical resistance.

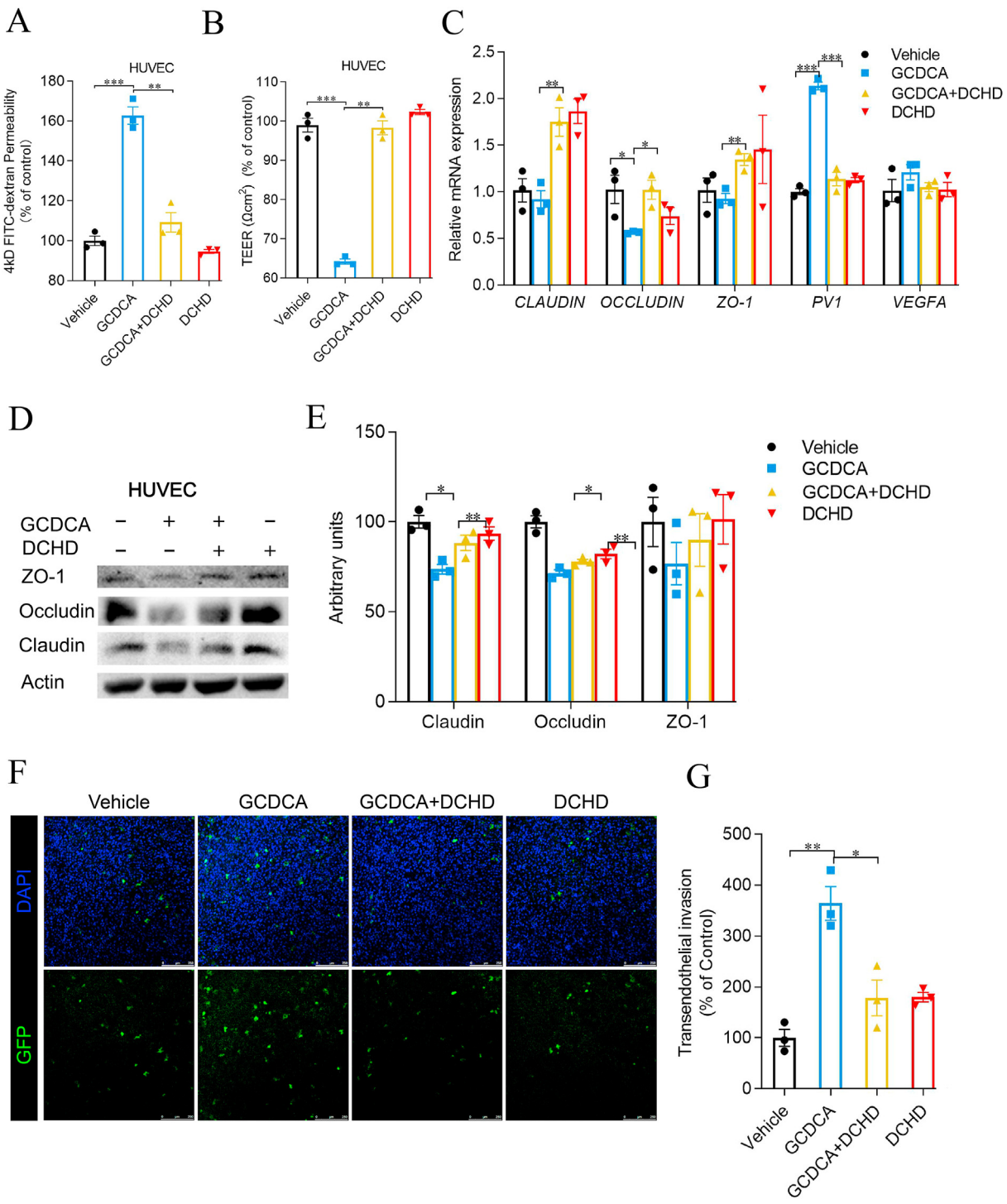

Figure 4. Dachaihu decoction inhibits glycochenodeoxycholic acid-induced permeabilization in cultured human umbilical vein endothelial cells. (A) FITC-dextran permeability in HUVECs treated with GCDCA and DCHD singly or in combination. (B) TEER analysis in HUVECs; results from three independent experiments. (C) qRT-PCR analysis of expression of TJ and vascular markers in HUVECs. (D) Western blot analysis of TJ proteins. (E) Densitometry of TJ proteins and control β-actin. (F) Invasion of GFP-expressing HCT-116 CRC cells across the HUVEC monolayer. GFP (green) and DNA staining (blue). Scale bar, 250 μm. (G) Quantitation of migrated GFP-HCT-116 cells in the lower Transwell chamber; results from three independent experiments. Mean ± SD, $^{*}P < 0.05$, $^{**}P < 0.01$, $^{***}P < 0.001$.CRC: Colorectal cancer; DCHD: Dachaihu decoction; FITC: Fluorescein-isothiocyanate-labeled; GCDCA: Glycochenodeoxycholic acid; GFP: Green fluorescent protein; HUVECs: Human umbilical vein endothelial cells; MFI: Mean fluorescence intensity; qRT-PCR: Quantitative real-time polymerase chain reaction; SD: Standard deviation; TEER: Transepithelial electrical resistance; TJ: Tight junction.

to aberrant lipid metabolism, which is often caused by hypernutrition-induced obesity and hyperlipidemia. Abnormal levels of lipids, including TG, cholesterol, and BAs induce liver metastasis in CRC and confer anticancer drug resistance through a number of mechanisms, contributing to high CRC mortality.[14] About 50% of patients with CRC develop more aggressive CRC liver metastasis during the course of the disease.[46] CRC liver metastasis begins with a few CRC cells that acquire the ability to escape the primary CRC and local migration and extravasation play key roles in the liver metastasis.[17] In this study, we modeled CRC metastasis in the presence of hyperlipidemia in mice to study the

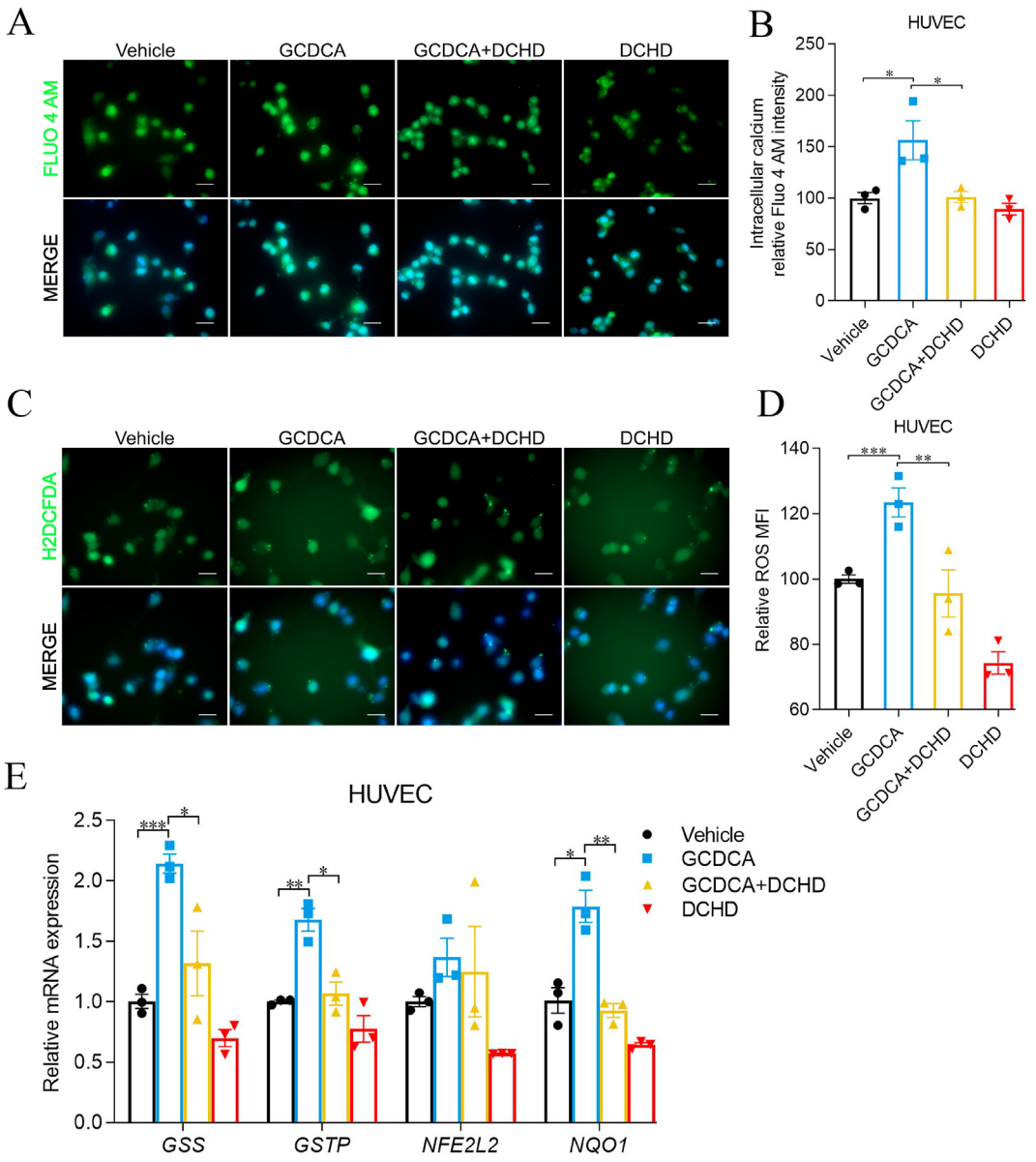

Figure 5. Dachaihu decoction prevents intracellular Ca^{2+} elevation and reactive oxygen species accumulation induced by glycochenodeoxycholic acid. (A) Live cell imaging of Fluo-4 AM (green) staining of intracellular Ca^{2+} in HUVECs after treatment with GCDCA alone or in combination with DCHD. Nuclei were stained with Hoechst 33342 (blue). Scale bar, 50 μm. (B) Quantitation of Fluo-4 AM intensity. (C) Live cell staining of ROS using H2DCFDA. Nuclei were stained with Hoechst 33342 (blue). Scale bar, 50 μm. (D) Quantitation of MFI for H2DCFDA. (E) qRT-PCR analysis of expression of oxidative stress response genes. Mean ± SD. $^{*}P < 0.05$, $^{**}P < 0.01$, $^{***}P < 0.001$.DCHD: Dachaihu decoction; GCDCA: Glycochenodeoxycholic acid; H2DCFDA: 2′,7′-dichlorodihydrofluorescein diacetate; HUVECs: Human umbilical vein endothelial cells; qRT-PCR: Quantitative real-time polymerase chain reaction; ROS: Reactive oxygen species; SD: Standard deviation.

specific effects of hypernutrition on CRC liver metastasis and in the attempt to find an effective treatment to prevent CRC metastasis to the liver. Our results showed that HFD induced obesity and hyperlipidemia, including elevation of blood TG and cholesterol levels. Cholesterol is recycled back to the liver and acts as a substrate to produce other lipids in the form of BAs. Increased blood lipids trigger disruption of BA metabolic homeostasis, and this may play a role in liver metastasis in CRC induced by hyperlipidemia.[11] Mechanistically, DCHD appeared to decrease liver metastasis in CRC by alleviating abnormal lipid metabolism. DCHD regulates BA metabolism and decreases BA levels. BAs induced liver metastasis in CRC. More importantly, DCHD downregulated the expression of genes involved in BA synthesis, uptake, and secretion in the liver, including *Cyp7a1*, *Cyp8b1a*, *Cyp27a1*, *Cyp7b1*, *Bsep*, *Ntcp*, *Baat*, and *Bacs*. In addition, DCHD decreased the expression of genes involved in BA absorption and secretion into the systemic circulation such as *Asbt*, *Mrp2*, *Osta*, and *Ostb* in terminal ileum enterocytes. Particularly, the expression of genes involved in primary C-BA synthesis and transport, including *Baat*, *Bacs*, and *Ntcp*, was downregulated following DCHD administration. Previous studies have demonstrated the deleterious effects of primary C-BAs, levels of which are notably increased in HFD-fed mice, in CRC development and metastasis.[40,47] Overall, the beneficial effects of DCHD are comparable to those of OCA, which is commonly used to treat lipid metabolic disorders. DCHD decreased HFD-induced body weight gain, but more importantly, DCHD mitigated hyperlipidemia and decreased the number of metastatic liver nodules in CRC. High doses of DCHD prolonged the OS of mice with CRC liver metastasis.

GVB disruption plays a key role in facilitating the entry of CRC tumor cells into the portal vein and subsequent dissemination via the hematogenous route, which enables liver metastasis.[18] Here, we showed that DCHD administration improved the intestinal morphology and reversed

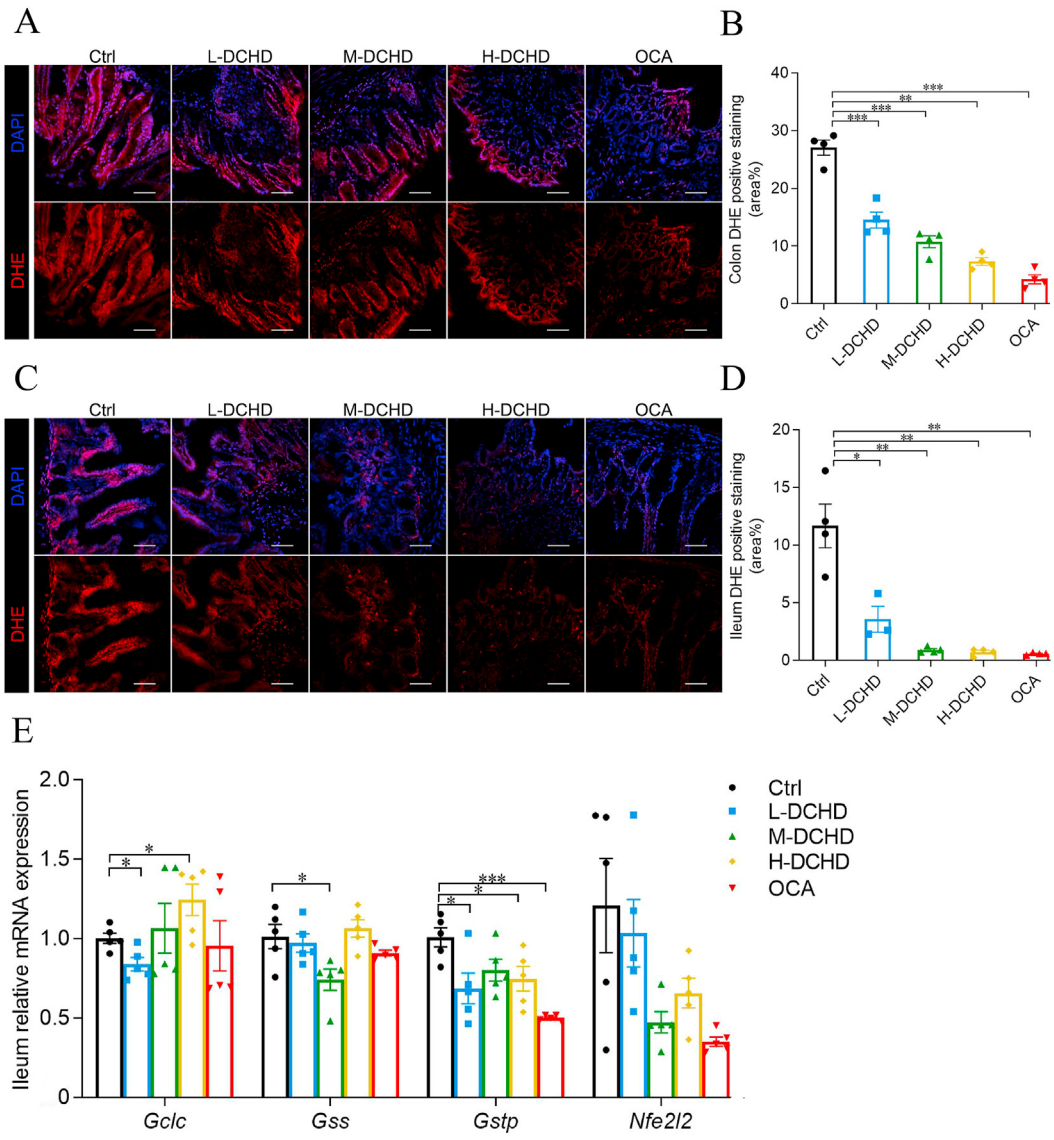

Figure 6. Dachaihu decoction inhibits high-fat-diet-induced reactive oxygen species accumulation in the colon and ileum of high-fat-diet-fed mice. (A) DHE staining of ROS (red) in colon sections of HFD-fed orthotopic CRC-bearing mice and DAPI staining (blue), Scale bar, 50 μm. (B) Quantitation of DHE positive area (%). $^{*}P < 0.05$, $^{**}P < 0.01$, $^{***}P < 0.001$. (C) DHE staining (red) and DAPI staining (blue) of ileum sections. Scale bar, 50 μm. (D) Quantitation of DHE positive area (%). $^{*}P < 0.05$, $^{**}P < 0.01$, $^{***}P < 0.001$. (E) qRT-PCR analysis of expression of oxidative stress response genes in the ileum. Means ± SD, $^{*}P < 0.05$, $^{**}P < 0.01$, $^{***}P < 0.001$. CRC: Colorectal cancer; DHE: Dihydroethidium; HFD: High-fat diet; ROS: Reactive oxygen species; qRT-PCR: Quantitative real-time polymerase chain reaction; SD: Standard deviation.

the decreased expression of mucus markers induced by HFD feeding, thus protecting the integrity of the gut barrier. Mechanistically, DCHD decreased GVB permeability by upregulating the expression of TJ proteins but downregulating PV-1 and VEGFA, resulting in the inhibition of CRC tumor cell movement via blood circulation. In addition, DCHD likely restores the function of LSECs by increasing liver ZO-1 expression, which is inhibited by HFD. Liver CD34 staining did not reveal significant morphological changes in liver LSECs, suggesting no or few apparent adverse effects of DCHD on the liver. Specialized LSECs with unique morphology and function facilitate interactions with circulating cancer cells and induce cancer cell liver colonization.[37] Therefore, DCHD likely prevents liver metastasis in CRC by maintaining the function of both the GVB and LSECs, with major effects on the intravasation and extravasation processes, respectively, in CRC metastasis. Of note, ZO-1 is not exclusively expressed in the tight junctions of LSECs; it is also expressed in the paracellular hepatocytes around the lumen of bile canaliculi.[38] To understand the effects of DCHD on the function of LSECs, more studies are needed, including the use of LSEC-specific markers. The molecular mechanism through which DCHD regulates TJ gene expression remains unclear and requires further investigation.

C-BAs interact with intestinal barrier cells including intestinal epithelial cells and the endothelium and disrupt this fundamental barrier, which can lead to the systemic entry of harmful entities, such as intestinal microbes and their metabolites, and initiation of tumor-promoting inflammation.[43,48] We demonstrated the effect of individual C-BAs in damaging the vascular barrier in HUVECs and found that GCDCA was the most potent BA in permeabilizing the HUVEC monolayer barrier, followed by TCA and TCDCA, with the least effects seen for GCA. DCHD treatment reversed HUVEC barrier disruption induced by GCDCA and increased the expression of TJ proteins. Similarly, DCHD reversed GVB impairment induced by individual BA treatments or HFD feeding *in vivo*. Thus, DCHD reverses the HFD-induced increase in GVB permeability caused by C-BAs.

Ca^{2+} and ROS are triggers that play a role in regulating TJ to control barrier permeability.[49] Our data showed that DCHD inhibited intracellular Ca^{2+} increase and ROS accumulation triggered by GCDCA *in vitro* at

3 h, much earlier than changes in gene expression observed at 24 h. Increased ROS levels initiate the oxidative stress response and the expression of glutathione metabolism-associated genes, such as *GSS* and *GSTP*, which are responsible for glutathione synthesis and utilization, respectively. In HUVECs, GCDCA increased *GSS* and *GSTP* expression, which was consistent with the induction of ROS accumulation and response to oxidative stress. DCHD reversed these effects of GCDCA.

We demonstrated that DCHD increases TJ protein expression and restores GVB integrity to inhibit CRC metastasis by inhibiting intracellular Ca^{2+} release and ROS accumulation; however, the components or combinations of active components in DCHD that mediate the beneficial effects remain unclear. This study did not address the functional ingredients of DCHD and their mechanisms of action, which is likely to be a major hurdle for clinical application. Although we did not observe any obvious adverse effects of DCHD at the tested doses, the therapeutic capability of DCHD and its potential side effects require further investigation, especially in the form of clinical studies.

Conclusion

Hyperlipidemia aggravates CRC liver metastasis, and a high percentage of patients with CRC have lipid metabolic disorders. Alleviating hyperlipidemia can efficiently inhibit liver metastasis in CRC. Our results indicate that DCHD controls Ca^{2+} flux and ROS accumulation to repair GVB disruption induced by BAs and hyperlipidemia and restores the expression of TJ proteins inhibited by BAs. In addition, DCHD alleviates hyperlipidemia to lower BA synthesis and transport, thus decreasing the adverse effects of BAs, such as GVB disruption. By controlling Ca^{2+} flux and ROS accumulation in endothelial cells as well as lowering levels of blood lipids, DCHD restores the GVB and prevents CRC tumor cell invasion. OCA, a synthetic derivative of an endogenous primary BA, has been approved by the Food and Drug Administration for the treatment of chronic liver diseases, including primary biliary cholangitis. OCA modulated BA metabolism by targeting the FXR. OCA has some side effects, including itching, fatigue, and abdominal pain.[50] DCHD not only has therapeutic potential for hyperlipidemia but is also cost-effective, and there have been no serious side effects reported for DCHD at the doses administered.[26] Apart from GVB protection and inhibition of CRC metastasis, the effects of DCHD and its active ingredients on primary tumor development, drug resistance, and gut bacteria homeostasis remain to be investigated, but even without these potential additional benefits, DCHD may represent a cost-effective formula for the prevention of hypernutrition-related CRC metastasis.

Funding

This work was supported by grants from the National Natural Science Foundation of China (No. 82003641) and the Beijing Natural Science Foundation (No.7222147).

Authors contribution

Ruolei Wang, Fengjing Jia, and Zhenguo Zhao performed the experiments and analyzed the data. Ruolei Wang wrote the original draft of this manuscript. Liqing Du and Lianheng Lu provided technical assistance and reviewed the manuscript. Dongkui Xu and Feng He conceptualized and supervised the study. Feng He designed the study and edited the manuscript. All authors have discussed and approved the manuscript.

Ethics statement

Institutional Review Board Statement: The study was conducted in accordance with the guidelines of the *Declaration of Helsinki* and approved by the Shanghai University of Traditional Chinese Medicine Animal Care Committee (Protocol code: PZSHUTCM220711017).

Data availability statement

The data and materials for this study are available upon reasonable request.

Conflict of interest

None.

Acknowledgments

We thank members of Dr. He's lab for helpful discussions and technical advice.

Appendix A. Supplementary data

Supplementary data to this article can be found online at https://doi.org/10.1016/j.cpt.2023.02.003.

References

1. Sung H, Ferlay J, Siegel RL, et al. Global Cancer Statistics 2020: GLOBOCAN Estimates of incidence and mortality worldwide for 36 cancers in 185 countries. *CA A Cancer J Clin.* 2021;71:209–249. https://doi.org/10.3322/caac.21660.
2. Brenner H, Kloor M, Pox CP. Colorectal cancer. *Lancet.* 2014;383:1490–1502. https://doi.org/10.1016/S0140-6736(13)61649-9.
3. Keum N, Giovannucci E. Global burden of colorectal cancer: emerging trends, risk factors and prevention strategies. *Nat Rev Gastroenterol Hepatol.* 2019;16:713–732. https://doi.org/10.1038/s41575-019-0189-8.
4. Yi H, Liao ZW, Chen JJ, et al. Genome variation in colorectal cancer patient with liver metastasis measured by whole-exome sequencing. *J Gastrointest Oncol.* 2021;12:507–515. https://doi.org/10.21037/jgo-21-9.
5. Wang Y, Guo H, He F. Circadian disruption: from mouse models to molecular mechanisms and cancer therapeutic targets. *Cancer Metastasis Rev.* 2022. https://doi.org/10.1007/s10555-022-10072-0.
6. Kim J, He F, Karin M. From liver fat to cancer: perils of the western diet. *Cancers.* 2021;13:1095. https://doi.org/10.3390/cancers13051095.
7. Liu PH, Wu K, Ng K, et al. Association of obesity with risk of early-onset colorectal cancer among women. *JAMA Oncol.* 2019;5:37–44. https://doi.org/10.1001/jamaoncol.2018.4280.
8. Yamashita S, Nishi M, Ikemoto T, et al. Clinical analysis of postoperative venous thromboembolism in Japanese patients after colorectal cancer surgery. *Surg Today.* 2021;51:1022–1027. https://doi.org/10.1007/s00595-020-02201-5.
9. Nakashima C, Shingo K, Fujiwara-Tani R, et al. Expression of long-chain fatty acid receptor GPR40 is associated with cancer progression in colorectal cancer: a retrospective study. *Oncol Lett.* 2018;15:8641–8646. https://doi.org/10.3892/ol.2018.8383.
10. Bagchi S, He Y, Zhang H, et al. CD1b-autoreactive T cells contribute to hyperlipidemia-induced skin inflammation in mice. *J Clin Invest.* 2017;127:2339–2352. https://doi.org/10.1172/JCI92217.
11. Jia W, Xie G, Jia W. Bile acid-microbiota crosstalk in gastrointestinal inflammation and carcinogenesis. *Nat Rev Gastroenterol Hepatol.* 2018;15:111–128. https://doi.org/10.1038/nrgastro.2017.119.
12. Li C, Wang Y, Liu D, et al. Squalene epoxidase drives cancer cell proliferation and promotes gut dysbiosis to accelerate colorectal carcinogenesis. *Gut.* 2022;71:2253–2265. https://doi.org/10.1136/gutjnl-2021-325851.
13. Yueh MF, He F, Chen C, et al. Triclosan leads to dysregulation of the metabolic regulator FGF21 exacerbating high fat diet-induced nonalcoholic fatty liver disease. *Proc Natl Acad Sci U S A.* 2020;117:31259–31266. https://doi.org/10.1073/pnas.2017129117.
14. Zhang Q, Deng T, Zhang H, et al. Adipocyte-derived exosomal MTTP suppresses ferroptosis and promotes chemoresistance in colorectal cancer. *Adv Sci.* 2022;9,e2203357. https://doi.org/10.1002/advs.202203357.
15. He F, Ru X, Wen T. NRF2, a transcription factor for stress response and beyond. *Int J Mol Sci.* 2020;21:4777. https://doi.org/10.3390/ijms21134777.
16. Pita-Fernandez S, Alhayek-Ai M, Gonzalez-Martin C, Lopez-Calvino B, Seoane-Pillado T, Pertega-Diaz S. Intensive follow-up strategies improve outcomes in nonmetastatic colorectal cancer patients after curative surgery: a systematic review and meta-analysis. *Ann Oncol.* 2015;26:644–656. https://doi.org/10.1093/annonc/mdu543.
17. Tsilimigras DI, Brodt P, Clavien PA, et al. Liver metastases. *Nat Rev Dis Prim.* 2021;7:27. https://doi.org/10.1038/s41572-021-00261-6.
18. Bertocchi A, Carloni S, Ravenda PS, et al. Gut vascular barrier impairment leads to intestinal bacteria dissemination and colorectal cancer metastasis to liver. *Cancer Cell.* 2021;39:708–724.e11. https://doi.org/10.1016/j.ccell.2021.03.004.
19. Sorribas M, Jakob MO, Yilmaz B, et al. FXR modulates the gut-vascular barrier by regulating the entry sites for bacterial translocation in experimental cirrhosis. *J Hepatol.* 2019;71:1126–1140. https://doi.org/10.1016/j.jhep.2019.06.017.
20. Gabitova-Cornell L, Surumbayeva A, Peri S, et al. Cholesterol pathway inhibition induces TGF-beta signaling to promote basal differentiation in pancreatic cancer. *Cancer Cell.* 2020;38:567–583. https://doi.org/10.1016/j.ccell.2020.08.015.

21. Siddiqui MS, Van Natta ML, Connelly MA, et al. Impact of obeticholic acid on the lipoprotein profile in patients with non-alcoholic steatohepatitis. *J Hepatol*. 2020;72:25–33. https://doi.org/10.1016/j.jhep.2019.10.006.
22. Cheng CS, Chen J, Tan HY, Wang N, Chen Z, Feng Y. Scutellaria baicalensis and cancer treatment: recent progress and perspectives in biomedical and clinical studies. *Am J Chin Med*. 2018;46:25–54. https://doi.org/10.1142/S0192415X18500027.
23. World Health Organization. *WHO global report on traditional and complementary medicine 2019*. World Health Organization; 2019. Available from: https://apps.who.int/iris/handle/10665/312342 [Last accessed on 1 May, 2022].
24. Duan LF, Xu XF, Zhu LJ, et al. Dachaihu decoction ameliorates pancreatic fibrosis by inhibiting macrophage infiltration in chronic pancreatitis. *World J Gastroenterol*. 2017;23:7242–7252. https://doi.org/10.3748/wjg.v23.i40.7242.
25. Cui H, Li Y, Wang Y, et al. Da-Chai-Hu decoction ameliorates high fat diet-induced nonalcoholic fatty liver disease through remodeling the gut microbiota and modulating the serum metabolism. *Front Pharmacol*. 2020;11, 584090. https://doi.org/10.3389/fphar.2020.584090.
26. Zhang Z, Leng Y, Fu X, et al. The efficacy and safety of dachaihu decoction in the treatment of type 2 diabetes mellitus: a systematic review and meta-analysis. *Front Pharmacol*. 2022;13, 918681. https://doi.org/10.3389/fphar.2022.918681.
27. Han K, Kwon O, Park HJ, Jung SY, Yang C, Son CG. Effect of Daesiho-tang on obesity with non-alcoholic fatty liver disease: a study protocol for a randomised, double-blind, placebo-controlled pilot trial. *Trials*. 2020;21:128. https://doi.org/10.1186/s13063-020-4068-y.
28. Yang JM, Sun Y, Wang M, et al. Regulatory effect of a Chinese herbal medicine formula on non-alcoholic fatty liver disease. *World J Gastroenterol*. 2019;25:5105–5119. https://doi.org/10.3748/wjg.v25.i34.5105.
29. Umemura A, He F, Taniguchi K, et al. p62, upregulated during preneoplasia, induces hepatocellular carcinogenesis by maintaining survival of stressed HCC-initiating cells. *Cancer Cell*. 2016;29:935–948. https://doi.org/10.1016/j.ccell.2016.04.006.
30. Kasashima H, Duran A, Cid-Diaz T, et al. Mouse model of colorectal cancer: orthotopic co-implantation of tumor and stroma cells in cecum and rectum. *STAR Protoc*. 2021;2, 100297. https://doi.org/10.1016/j.xpro.2021.100297.
31. Zhang L, Bu P. Generation of an orthotopic mouse model to study colorectal cancer metastasis. *STAR Protoc*. 2021;2, 100792. https://doi.org/10.1016/j.xpro.2021.100792.
32. He F, Antonucci L, Yamachika S, et al. NRF2 activates growth factor genes and downstream AKT signaling to induce mouse and human hepatomegaly. *J Hepatol*. 2020;72:1182–1195. https://doi.org/10.1016/j.jhep.2020.01.023.
33. Shan B, Wang X, Wu Y, et al. The metabolic ER stress sensor IRE1alpha suppresses alternative activation of macrophages and impairs energy expenditure in obesity. *Nat Immunol*. 2017;18:519–529. https://doi.org/10.1038/ni.3709.
34. Zhou J, Huang N, Guo Y, et al. Combined obeticholic acid and apoptosis inhibitor treatment alleviates liver fibrosis. *Acta Pharm Sin B*. 2019;9:526–536. https://doi.org/10.1016/j.apsb.2018.11.004.
35. Mouries J, Brescia P, Silvestri A, et al. Microbiota-driven gut vascular barrier disruption is a prerequisite for non-alcoholic steatohepatitis development. *J Hepatol*. 2019;71:1216–1228. https://doi.org/10.1016/j.jhep.2019.08.005.
36. Spadoni I, Pietrelli A, Pesole G, Rescigno M. Gene expression profile of endothelial cells during perturbation of the gut vascular barrier. *Gut Microb*. 2016;7:540–548. https://doi.org/10.1080/19490976.2016.1239681.
37. Yang M, Zhang C. The role of liver sinusoidal endothelial cells in cancer liver metastasis. *Am J Cancer Res*. 2021;11:1845–1860.
38. Boyer JL. Tight junctions in normal and cholestatic liver: does the paracellular pathway have functional significance? *Hepatology*. 1983;3:614–617. https://doi.org/10.1002/hep.1840030423.
39. Ocvirk S, O'Keefe SJD. Dietary fat, bile acid metabolism and colorectal cancer. *Semin Cancer Biol*. 2021;73:347–355. https://doi.org/10.1016/j.semcancer.2020.10.003.
40. Zheng Z, Wei J, Hou X, et al. A High hepatic uptake of conjugated bile acids promotes colorectal cancer-associated liver metastasis. *Cells*. 2022;11:3810. https://doi.org/10.3390/cells11233810.
41. Sun L, Cai J, Gonzalez FJ. The role of farnesoid X receptor in metabolic diseases, and gastrointestinal and liver cancer. *Nat Rev Gastroenterol Hepatol*. 2021;18:335–347. https://doi.org/10.1038/s41575-020-00404-2.
42. Rigor RR, Shen Q, Pivetti CD, Wu MH, Yuan SY. Myosin light chain kinase signaling in endothelial barrier dysfunction. *Med Res Rev*. 2013;33:911–933. https://doi.org/10.1002/med.21270.
43. Hegyi P, Maleth J, Walters JR, Hofmann AF, Keely SJ. Guts and gall: bile acids in regulation of intestinal epithelial function in health and disease. *Physiol Rev*. 2018;98:1983–2023. https://doi.org/10.1152/physrev.00054.2017.
44. Huang SF, Othman A, Koshkin A, et al. Astrocyte glutathione maintains endothelial barrier stability. *Redox Biol*. 2020;34, 101576. https://doi.org/10.1016/j.redox.2020.101576.
45. He F, Antonucci L, Karin M. NRF2 as a regulator of cell metabolism and inflammation in cancer. *Carcinogenesis*. 2020;41:405–416. https://doi.org/10.1093/carcin/bgaa039.
46. Zhou H, Liu Z, Wang Y, et al. Colorectal liver metastasis: molecular mechanism and interventional therapy. *Signal Transduct Targeted Ther*. 2022;7:70. https://doi.org/10.1038/s41392-022-00922-2.
47. Fu T, Coulter S, Yoshihara E, et al. FXR regulates intestinal cancer stem cell proliferation. *Cell*. 2019;176:1098–1112 e18. https://doi.org/10.1016/j.cell.2019.01.036.
48. Jia F, Yu Q, Zhao L, Shen Y, Guo H, He F. Sodium new houttuyfonate inhibits cancer-promoting fusobacterium nucleatum (Fn) to reduce colorectal cancer progression. *Cancers*. 2022;14:6111. https://doi.org/10.3390/cancers14246111.
49. Brescia P, Rescigno M. The gut vascular barrier: a new player in the gut-liver-brain axis. *Trends Mol Med*. 2021;27:844–855. https://doi.org/10.1016/j.molmed.2021.06.007.
50. Kowdley KV, Vuppalanchi R, Levy C, et al. A randomized, placebo-controlled, phase II study of obeticholic acid for primary sclerosing cholangitis. *J Hepatol*. 2020;73:94–101. https://doi.org/10.1016/j.jhep.2020.02.033.